JGR Planets

RESEARCH ARTICLE

10.1029/2024JE008621

Influence of the Earthward and Tailward Ion Flows on the Lunar Surface Water in the Magnetotail

H. Z. Wang[1,2], Q. Q. Shi[1,2], J. Zhang[1], L. H. Xie[2], C. Yue[3], R. L. Guo[1], Y. Chen[1], W. L. Liu[4], T. Pitkänen[1,5], J.-S. Park[1], A. W. Degeling[1], A. M. Tian[1], T. L. Chen[6], S. Q. Zhao[7], K. X. Li[1], Y. Fu[1], J. Chen[1], C. Xiao[8], W. S. Shang[1], J. Liu[9], Q. G. Zong[3,10], and S. Y. Fu[3]

[1]Shandong Key Laboratory of Space Environment and Exploration Technology, Institute of Space Sciences, School of Space Science and Technology, Shandong University, Weihai, China, [2]State Key Laboratory of Solar Activity and Space Weather, National Space Science Center, Chinese Academy of Sciences, Beijing, China, [3]School of Earth and Space Sciences, Institute of Space Physics and Applied Technology, Peking University, Beijing, China, [4]School of Space and Environment, Beihang University, Beijing, China, [5]Department of Physics, Umeå University, Umeå, Sweden, [6]The Key Laboratory of Cosmic Rays, Tibet University, Ministry of Education, Lhasa, China, [7]Deutsches Elektronen-Synchrotron DESY, Platanenallee 6, Zeuthen, Germany, [8]College of Advanced Interdisciplinary Studies, National University of Defense Technology, Changsha, China, [9]Department of Physics, University of Alberta, Edmonton, AB, Canada, [10]State Key Laboratory of Lunar and Planetary Sciences, Macau University of Science and Technology, Taipa, China

Abstract Earth wind, namely the particles from the Earth's magnetotail, is an important source of lunar water. Besides tailward flow incident on the lunar nearside when the Moon is in the magnetotail, there exists earthward flow bombarding the farside, affecting the distribution and preservation of lunar water. In this study, we determine the incident fluxes of both the tailward and earthward flows on the lunar surface with the ARTEMIS observations and examine their influences on the concentration and migration of lunar surface water and its reservation in the polar regions using Monte Carlo modeling. It is found that water molecules produced by the earthward flow can stay longer on the surface than those produced by the tailward flow. Our results suggest that the evolution of the Earth's magnetosphere can be inferred from Earth wind particles implanted in the soils of both the lunar nearside and farside.

Plain Language Summary The Earth wind, namely the particles from the Earth's magnetotail, is one of several non-negligible sources of lunar surface water. Previous studies on lunar water have considered only the lunar nearside data when the Moon is in the magnetotail. However, the lunar farside is also implanted by the earthward flow in the magnetotail. It is critical for understanding energy and mass transport in the Earth-Moon system and the production, migration, and preservation of lunar water. In this work, we examine the influence of the tailward and earthward flows on lunar water molecules using a Monte Carlo model with input parameters determined from the ARTEMIS observations. The results show that the water molecules produced by the earthward flow can stay at the lunar surface longer than those produced by the tailward flow due to the low temperature on the lunar farside surface in the magnetotail. Our results suggest that the evolution of the Earth's magnetosphere can be inferred from the Earth wind particles constantly implanted into the lunar soils of both the nearside and farside surfaces. Future missions and studies, especially those focusing on the lunar farside, can provide essential clues about how the Earth wind interacts with the lunar surface.

Key Points:

- We examine the influence of the tailward and earthward flows on lunar surface water molecules using ARTEMIS data and a Monte Carlo model
- The occurrence rate of earthward flow implanted on the lunar farside exceeds that of tailward flow implanted on the lunar nearside
- Water molecules produced by the earthward flow show longer residence time on the lunar farside surface when the Moon is in the magnetotail

Correspondence to:

Q. Q. Shi and J. Zhang,
sqq@sdu.edu.cn;
zhang_jiang@sdu.edu.cn

Citation:

Wang, H. Z., Shi, Q. Q., Zhang, J., Xie, L. H., Yue, C., Guo, R. L., et al. (2025). Influence of the earthward and tailward ion flows on the lunar surface water in the magnetotail. *Journal of Geophysical Research: Planets*, *130*, e2024JE008621. https://doi.org/10.1029/2024JE008621

Received 31 JUL 2024
Accepted 15 NOV 2025

Author Contributions:

Conceptualization: H. Z. Wang, Q. Q. Shi, J. Zhang, L. H. Xie
Data curation: H. Z. Wang
Formal analysis: H. Z. Wang, W. L. Liu, A. M. Tian, S. Q. Zhao, J. Chen, C. Xiao, W. S. Shang, S. Y. Fu
Funding acquisition: H. Z. Wang, Q. Q. Shi
Investigation: H. Z. Wang, R. L. Guo, T. Pitkänen, J.-S. Park, A. M. Tian, S. Q. Zhao, C. Xiao
Methodology: H. Z. Wang, J. Zhang, L. H. Xie, C. Yue, S. Y. Fu
Project administration: H. Z. Wang
Software: H. Z. Wang, T. Pitkänen, J.-S. Park, W. S. Shang, J. Liu, S. Y. Fu
Supervision: Q. Q. Shi, J. Zhang
Validation: H. Z. Wang, J. Zhang, J. Chen, S. Y. Fu
Visualization: H. Z. Wang

1. Introduction

Understanding the distribution and migration of surficial water on the Moon plays a crucial role in studying the lunar exosphere and its volatile evolution. Water-related signals have been detected on the lunar surface through characteristic absorption features at 3 μm and 6 μm wavelengths by different independent instruments (Bandfield et al., 2018; Farrell et al., 2017; Hendrix et al., 2019; Honniball et al., 2021; Kramer et al., 2011; Li & Milliken, 2017; McCord et al., 2011; Pieters et al., 2009; Sunshine et al., 2009; Watson et al., 1961; Wöhler et al., 2017). The observed 2.8 μm OH/H_2O feature on the lunar surface shows diurnal variation, indicating a dynamic balance between continuous production by the solar wind, and loss processes (Sunshine et al., 2009). Further evidence that supports water production by the solar wind is the lunar surface OH/H_2O abundance decrease within magnetic anomalies, which is interpreted as the solar wind being deflected by the magnetic anomalies (Kramer et al., 2011; Li & Garrick Bethell, 2019). Thus, the interaction between solar wind protons and

Writing – original draft: H. Z. Wang
Writing – review & editing: H. Z. Wang, Q. Q. Shi, J. Zhang, L. H. Xie, C. Yue, R. L. Guo, Y. Chen, W. L. Liu, T. Pitkänen, J.-S. Park, A. W. Degeling, T. L. Chen, S. Q. Zhao, J. Chen, Q. G. Zong, S. Y. Fu

the uppermost surface of lunar mineral grains was suggested as one of the possible mechanisms for the formation of OH/H_2O on the lunar surface (Bandfield et al., 2018; Farrell et al., 2017; Hendrix et al., 2019; Kramer et al., 2011; Li & Milliken, 2017; McCord et al., 2011; Pieters et al., 2009; Sunshine et al., 2009; Watson et al., 1961; Wöhler et al., 2017). This production process has also been confirmed by lunar sample analyses and laboratory ion irradiation experiments (Djouadi et al., 2011; Ichimura et al., 2012; Schaible & Baragiola, 2014; Tang et al., 2012; Zeng et al., 2021).

The Moon is exposed to various plasma environments along its orbit. Although the Moon spends most of its time in the variable solar wind, it also spends 3–5 days every month within the Earth's magnetotail, which is filled with terrestrial magnetospheric plasma. The magnetotail ions consist of not only protons originating from the solar wind and oxygen but also other heavier ions escaping from the Earth's ionosphere (including O^+, O_2^+, N^+, NO^+, etc.), which are collectively termed the Earth wind (Ozima et al., 2005). The Earth wind contents are highly dynamic and significantly affected by geomagnetic field reversals and geomagnetic disturbances (Fu et al., 2001; Wei et al., 2014; Yue et al., 2018). The Earth wind ions of ionospheric origin are efficiently transported to lunar orbit along magnetic field lines and have been observed there by Kaguya, Geotail, and ARTEMIS missions (Fu et al., 2001; Poppe et al., 2016; Seki et al., 2001; Terada et al., 2017; Zong et al., 1998). Both Chandrayaan-1 M^3 (Moon Mineralogy Mapper) and LRO LAMP (Lyman Alpha Mapping Project) observations suggest that the lunar surface water content does not decrease when the Moon enters the magnetotail, where the solar wind is shielded by the Earth's magnetic field (Hendrix et al., 2019; Wang et al., 2021). The Earth wind has been proposed as a possible contributor to the lunar surface water when the Moon is in the Earth's magnetotail (Wang et al., 2021). More recently, an association between the formation of lunar surface water during magnetotail crossings and magnetospheric plasma sheet properties was also proposed (Li et al., 2023).

Investigation of the characteristics and possible influence of particles in the magnetotail to the production of lunar water is very useful for us to understand the energy and mass transport in the Earth-Moon system. Wei et al. (2020) hypothesized that the evolution of the Earth's magnetosphere and atmosphere can be inferred by examining the implanted particles in the lunar soil from both the nearside and farside during lunar geological history. Except for the plasma background in the Earth wind, fast tailward and earthward ion flows from near-Earth and distant reconnection X lines, respectively, are also observed when the Moon passes through the magnetotail, both of which could influence the lunar surface. Indeed, fast plasma flows in the magnetotail have been observed within $66\ R_E < X_{GSM} < 9\ R_E$ (where GSM stands for the geocentric solar magnetospheric coordinate system), including lunar orbit by the Active Magnetospheric Particle Tracer Explorers/Ion Release Module (AMPTE/IRM), ISEE, Geotail, Cluster, and ARTEMIS satellite measurements (Angelopoulos et al., 1992, 1994; Baumjohann et al., 1990; Kiehas et al., 2018; Nagai et al., 1998; Zhang et al., 2015). Kiehas et al. (2018) reported that there are many fast earthward flows emanating from beyond lunar orbit using 5 years of ARTEMIS data, and suggested that near-Earth and mid-tail reconnection are equally probable to occur on either side of the ARTEMIS down-tail distance. In addition, hot ion flows (with energies of 2–5 keV) were also observed by the two THEMIS spacecraft before they inserted into lunar orbit in the distant magnetotail between lunar orbit and $200\ R_E$, and an X line was identified at around $80\ R_E$ distance (Artemyev et al., 2017). An X-line location beyond lunar orbit will generate fast earthward flows, which will implant into the lunar regolith and produce a sunward-oriented lunar wake in the magnetotail (Harnett et al., 2013; Ma et al., 2015). However, the possible influence of earthward and tailward flows on the lunar surface water remains unanswered. An outstanding challenge is a lack of data on the abundance of water on the lunar farside when the Moon was in the magnetotail. This can be mitigated using physics-based modeling and simulation, informed by available ARTEMIS observations. Previous studies have simulated the transport of water molecules on the lunar surface by a Monte Carlo model when the Moon is in the solar wind (Schörghofer, 2014; Schörghofer et al., 2017).

In order to answer this question, in this study, our motivation is to examine the influence of the tailward and earthward flows on the lunar surface water molecules using a water migration model with input parameters determined from the ARTEMIS observations. We statistically examine the occurrence rate of earthward/tailward flows ($|Vx| > 30$ km/s) within the Earth's magnetosphere using measurements around the Moon by the ARTEMIS satellite over an approximately 11-year period from January 2011 to January 2022. Then, we investigate the influence of the earthward/tailward flows on the lunar surface water molecules using a Monte Carlo model according to the ARTEMIS statistical results. The rest of this paper is structured as follows: In Section 2, we present the earthward and tailward flow events. In Section 3, we provide the statistical results of earthward/tailward flows and the modeling results. Finally, the discussion and conclusion of this paper are provided in Section 4 and 5.

2. Data Set and Simulation Methods

2.1. Data Set

The ARTEMIS mission (Angelopoulos, 2011; Sibeck et al., 2011) is the first dual spacecraft (ARTEMIS P1 and P2) mission designed to conduct studies on the near-Moon space environment along a lunar orbit. Since 2011, these two identical probes have been orbiting the Moon with an orbital period of about 26 hr. In this study, we use magnetic field and plasma (with energy ranges of several eV to 25 keV for ions and of several eV to 30 keV for electrons) data from Flux Gate Magnetometer (FGM) and Electrostatic Analyzer (ESA), respectively (Auster et al., 2008; McFadden et al., 2008), onboard ARTEMIS P1 to identify the earthward and tailward flow events in the magnetotail lunar orbit and examine their occurrence rates and energy spectra. Over the course of a lunar orbit, the ARTEMIS probes observe various plasma environments in the regions produced by the solar wind-magnetosphere interaction, such as the pristine solar wind, magnetosheath, and magnetotail. When the Moon transits from the solar wind to the magnetosheath, the plasma ion temperature typically increases from 10 to 40 eV, while the plasma velocity decreases from 400 500 km/s to 200 300 km/s. The plasma ion temperature further increases to 1,000 eV and the plasma density decreases when the Moon crosses the magnetopause and enters the plasma sheet in the magnetotail (Gencturk Akay et al., 2019; Liuzzo et al., 2022; Poppe et al., 2018). Using these characteristics as criteria, we identified 136 passages of the Moon through the magnetotail from January 2011 to January 2022.

The magnetotail near lunar orbit can be further divided into three different regions (i.e., the plasma sheet, the plasma sheet boundary layer, and the tail lobes) depending on the ion plasma beta (beta $2\mu_0 n k_B T$ B^2, where μ_0 is the vacuum permeability, n the ion number density, k_B the Boltzmann constant, T the ion average temperature, and B the magnitude of the magnetic field). The lobes are characterized by low number densities ($n < 0.1$ cm ^{3}) and strong magnetic field ($|B|$ 10 nT), while the plasma sheet is characterized by high number densities (n 0.1 cm ^{3}) and weak magnetic field ($|B| < 4$ nT) (Liuzzo et al., 2022). Correspondingly, the plasma beta values is typically greater than 1 in the plasma sheet, while below 0.05 in the lobes, and between these values in the plasma sheet boundary layer.

The velocity selection criteria used in previous statistical studies of plasma flows in the near-Earth magnetotail vary according to the purpose of the studies. For instance, the original definition of fast bursty bulk flows (BBFs) in the tail plasma sheet included a time segment of ion flow magnitude >100 km/s with at least one sample >400 km/s (Angelopoulos et al., 1992, 1994; Cao et al., 2006). When investigating the average tail ion flow patterns, a threshold of 200 km/s has often been used to divide the measurements into fast and slow flows (Chong et al., 2022; Kissinger et al., 2012; Pitkänen et al., 2019). The same threshold has also been applied to identify BBFs (Pitkänen et al., 2017; Zhang et al., 2016). Kiehas et al. (2018) studied the magnetotail fast flows using ion velocity data measured by the ARTEMIS probes in the mid-magnetotail at the lunar distance. They investigated the occurrence of ion flows at these distances using different threshold values ranging from 100 km/s to 400 km/s. Here, we identified the earthward flow events by using a threshold of Vx > 30 km/s for the time segments of the ion flow, whereas the tailward flow events were selected by Vx < 30 km/s. The implantation rate and the implantation depth into the lunar soil grain depend on various conditions such as the energy of the incident ions, the angle of incident ions from the target surface, and the composition of the target surface (Farrell et al., 2017). According to the modeling of proton implantation into silica by SRIM (The Stopping and Range of Ions in Matter) (Ziegler et al., 2010), the implantation rate of protons slower than 30 km/s is lower than 60%, and the implantation depth of these particles is extremely shallow. Therefore, these implanted protons can thermally diffuse out immediately and hardly contribute to water production within lunar mineral grains. The 30 km/s threshold was selected for the flows to have a finite magnitude at their lower limit, which we consider sufficient to ensure that the flows can implant into the lunar surface. Then, we further categorize the flow events into different subsets using various velocity thresholds (|Vx| > 30, 100, 200, 300, 400 km/s) in order to study the occurrence rate of flows with velocity. In addition, we use the following criteria to avoid magnetosheath samples: Ti > 300 eV and $n < 0.5$ cm ^{3} (Kiehas et al., 2018). The GSM coordinate system is used throughout this study. We then calculate the median energy spectrum and mean monthly time durations of earthward and tailward flow events (|Vx| > 30 km/s) from ARTEMIS observations.

2.2. Simulation Method

Previous studies have simulated the transport of water molecules on the lunar surface by a Monte Carlo model (Butler, 1997; Crider & Vondrak, 2000, 2002; Schörghofer, 2014). The transport is hypothesized to occur through random ballistic hops between the surface and the exosphere. Here, we use the Monte Carlo model for the random migration of water molecules on the lunar surface, which is available at github.com/nschorgh/Planetary-Code-Collection (Schörghofer, 2014, 2024; Schörghofer et al., 2017).

In previous studies, the water molecules were assumed to be produced directly in the daytime sector of the Moon by the continuous implantation of the solar wind protons (Schörghofer, 2014; Schörghofer et al., 2017). In this work, on the other hand, we assume that the water molecules are continuously generated on the lunar nearside by the tailward flow, while the water molecules are continuously generated on the lunar farside by the earthward flow when the Moon is in the magnetotail. The earthward flow and tailward flow implanted on the lunar surface have a cosine dependence with the lunar latitude and longitude. Moreover, the number of water molecules produced on the lunar farside surface and that produced on the nearside surface are assumed to be proportional to the flux of the earthward flow and that of the tailward flow, respectively.

As described by Schörghofer (Schörghofer, 2014; Schörghofer et al., 2017), individual water molecules on the lunar surface are launched with Gaussian-distributed Cartesian velocity components and thermal speeds appropriate for the local surface temperature. The lunar surface temperature is obtained from a one-dimensional thermal model (Vasavada et al., 2012). Water molecules hop at high surface temperatures while they reside on the surface at low temperatures, and temperature determines the residence time of water molecules on the surface, which is negligible on most of the lunar dayside and very long on most of the lunar nightside. The residence time of water molecules on the surface depends on the surface temperature T and on the adsorbate density θ (number of H_2O molecules per area), which is calculated by $\tau \quad \theta_m \ E \ T, \theta$, where $\theta_m \quad 10^{19}$ m ^{2} is the value of θ required for a complete monolayer of water molecules, E is the sublimation flux of ice as function of T and θ, T is the lunar surface temperature, and θ is the number of water molecules per unit area (Schörghofer, 2014).

The permanently shadowed regions near lunar poles are also called cold traps or cold-trapped regions (Schörghofer, 2014; Schörghofer et al., 2017). In the simulation, both photo-destruction and cold trapping by the permanently shadowed regions on the lunar surface are considered as dominant loss mechanisms of water molecule migration. The loss process of gravitational escape is also included in the simulation, although most molecules cannot exceed the escape velocity of the Moon. On the lunar dayside, the water molecules are lost in flight by photo-destruction with a total rate of 1.26 $\quad 10^{5}$ s ^{1} (Crovisier, 1989). Events are scheduled and processed until each molecule is destroyed or lost, or until its landing or launch time is beyond the next thermal model time step (set to 1 hour), whereupon the surface temperatures are updated.

3. Identification of Earthward and Tailward Flow Events in the Magnetotail

In this study, we use magnetic field and plasma data (with energy ranges of several eV to 25 keV for ions and of several eV to 30 keV for electrons) measured from the FGM and ESA instruments, respectively (Auster et al., 2008; McFadden et al., 2008), onboard ARTEMIS P1 to identify the earthward and tailward flow events in the magnetotail lunar orbit and examine their occurrence rates and energy spectra. Figure 1 shows examples of an earthward flow event (Figures 1a–1g) and a tailward flow event (Figures 1h–1n) in the magnetotail lunar orbits identified by using the plasma and magnetic field data obtained by the ARTEMIS P1 spacecraft. Figure 1a indicates that between 13:33:09 UT and 13:37:05 UT on 11 September 2011 (denoted by two vertical pink dashed lines), the ARTEMIS P1 detected an earthward flow event characterized by unexpected changes in the X component of the ion velocity of up to several hundred km/s from the surroundings (where Vx $\quad$ 0 km/s) at $P_{\mathrm{GSM}} \quad [\ 62.0, 12.3, \quad 1.0]\ R_E$. The ARTEMIS P1 also detected a tailward flow event showing abrupt changes in the magnitude of the X component of the ion velocity (reaching up to several hundred km/s from 0 km/s) at $P_{\mathrm{GSM}} \quad [\ 60.2, 10.3, 2.1]\ R_E$ between 20:34:40 UT and 20:37:02 UT on 09 November 2011, which can be seen in Figure 1g.

During each event, the X component of velocity gradually increases from zero to several hundred km/s. Simultaneously, the ion density and temperature increase. The differential energy fluxes for ions (in the energy range of several hundred eV to 10 keV) and electrons (in the energy range of $\quad$ 100 eV to $\quad$ 1 keV) both increase.

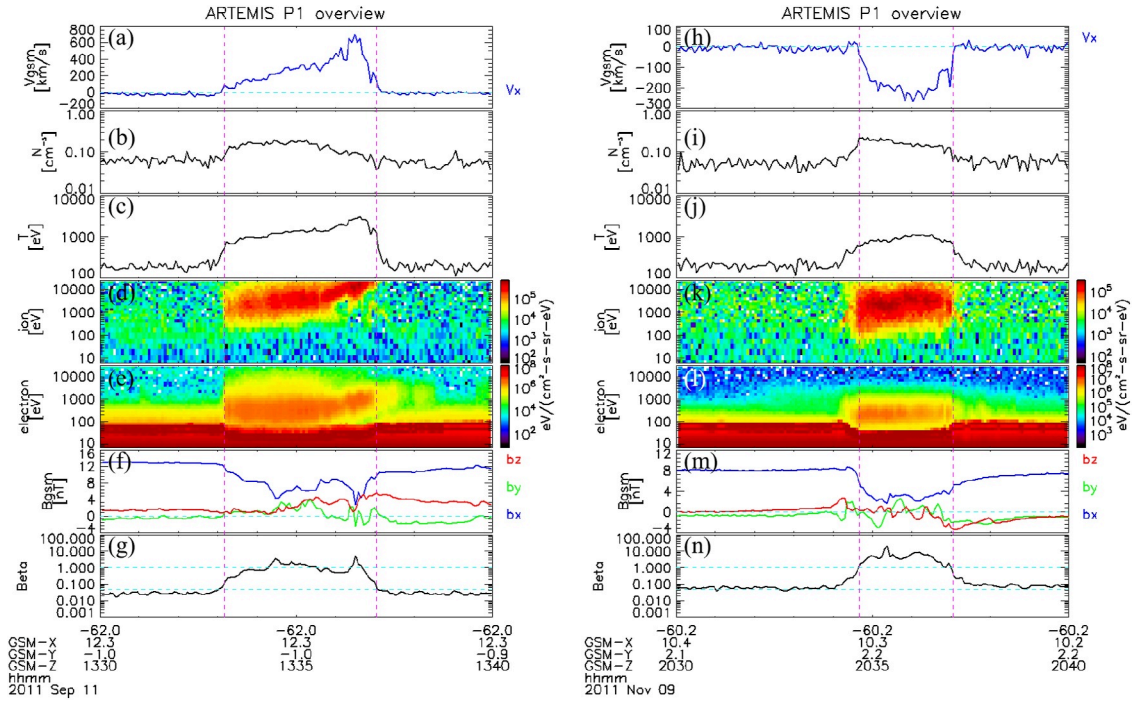

Figure 1. Overviews of (a–g) an earthward flow event and (h–n) a tailward flow event observed by the ARTEMIS-P1 spacecraft in the magnetotail (between pink dashed lines). The panels from top to bottom show plasma velocity, density, temperature, ion energy spectrum, electron energy spectrum, magnetic field, and ion plasma beta. The blue horizontal dashed line in panels a and b and panels (h and i) are horizontal zero-lines. The dashed blue line in panels g and n indicates 0.05 and 1.

The combined effect of the decrease in the magnitude of the magnetic field and the increase in the number density and temperature for ions leads to an abrupt increase of the ion plasma beta, which can be seen in the last panels of Figure 1 for both the earthward and tailward flow events.

4. Results

To exclude the effect of the spacecraft trajectory, the occurrence rates of the earthward and tailward flow events were calculated by dividing the numbers of data points in the earthward and tailward flow events by the total number of the data points of the ARTEMIS satellite orbits in the magnetotail, binned in 5 R_E intervals in Y_{GSM}. Figure 2 shows the occurrence rates of earthward and tailward flows according to Y_{GSM} for different velocity thresholds (|Vx| > 30, 100, 200, 300, and 400 km/s). We find that the occurrence rate of the earthward flows is generally higher than the tailward flows in the tail region of $10\ R_E < Y_{GSM} < 10\ R_E$ when low velocities are included (Figures 2a–2c vs. Figures 2f–2h), while the occurrence rate of the tailward flows is higher in $0\ R_E < Y_{GSM} < 10\ R_E$ when |Vx| is greater than 400 km/s (Figure 2e vs. Figure 2j). This is consistent with the results in Kiehas et al. (2018). Kiehas et al. (2018) pointed out that the tailward flows observed by ARTEMIS originate from the near-Earth region, while the earthward flows observed by ARTEMIS originate from the distant tail region. The magnetic field strength decreases with downtail distance, resulting in a lower reconnection outflow velocity with downtail distance. Therefore, comparatively lower (higher) flow speeds in the earthward (tailward) flows can be expected (Kiehas et al., 2018).

A comparison of the occurrence rates in the dusk sector and dawn sectors further reveals that the occurrence rate of the earthward flows is generally higher on the dawnside at velocities of 30 km/s < Vx < 400 km/s (Figures 2a–2d), while the occurrence rate of the earthward flows has no obvious asymmetry at velocities of Vx > 400 km/s (Figure 2e). On the other hand, the occurrence rate of the tailward flows has no obvious asymmetry at velocities 200 km/s < Vx < 30 km/s (Figures 2f and 2g), while the occurrence rate of the tailward flows at velocities of Vx < 200 km/s is higher on the duskside (Figures 2h–2j). Because the fast earthward flows have been suggested to be generated via distant tail magnetic reconnection, the symmetrical occurrence rate of the high-velocity earthward flows indicates that the distant reconnection *X* line is symmetrically active both in the dusk and dawn sectors (Kiehas et al., 2018). The occurrence rate of the tailward flows has no obvious asymmetry at low

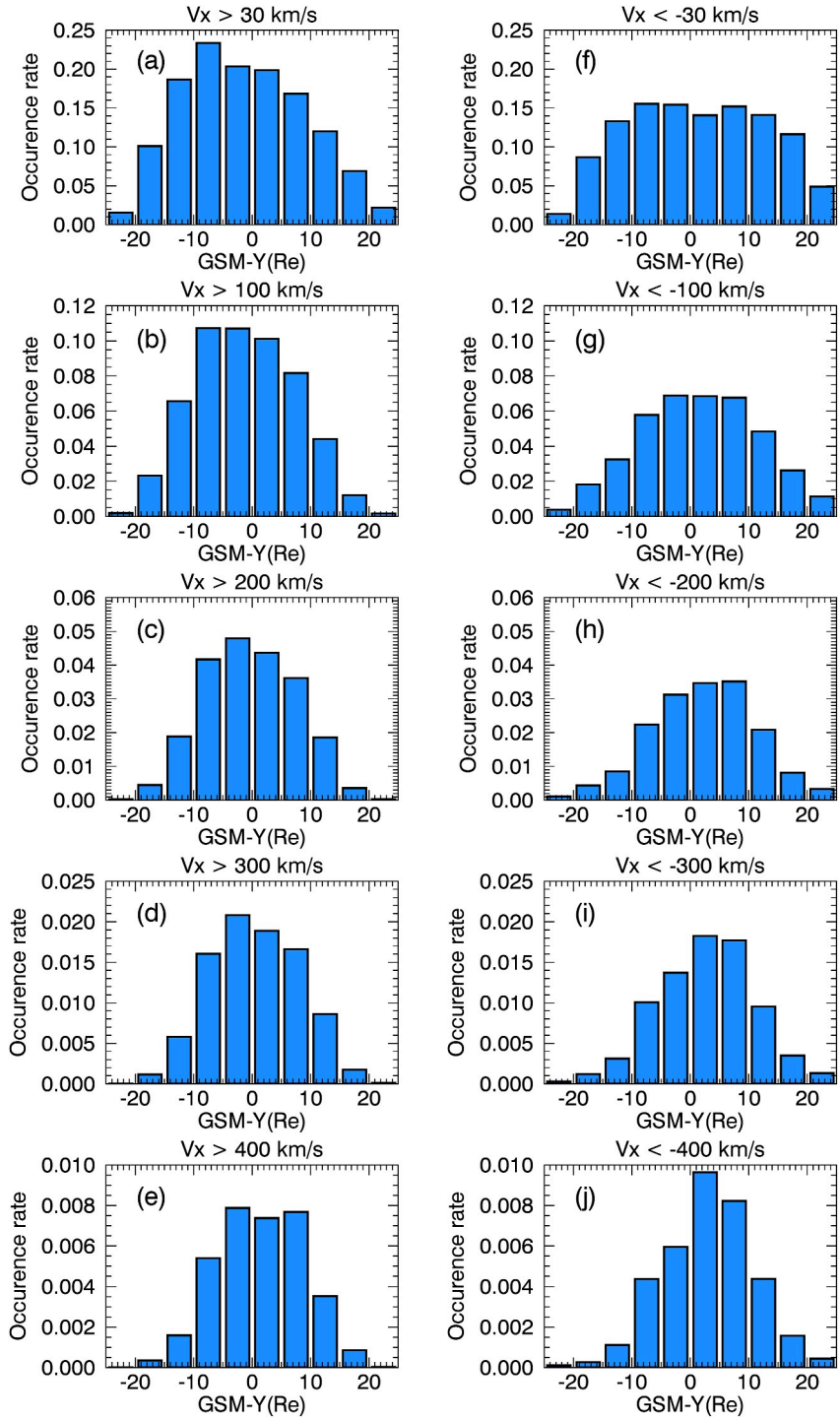

Figure 2. Occurrence rates of (a–e) earthward flows and (f–j) tailward flows as a function of Y_{GSM} for different velocity thresholds.

velocity. However, the occurrence rate of the tailward flows is higher on the duskside at large velocities, which is consistent with the result in Kiehas et al. (2018). This dawn-dusk asymmetry may be caused by the stronger Hall effect on the duskside, making magnetic reconnection more favorable to occur in the dusk sector (Lu et al., 2016). Nagai et al. (1998) inferred from the Geotail measurements that a typical location of the magnetic reconnection for substorm onsets appears in the pre-midnight sector of the plasma sheet at $30\ R_E < X_{GSM} < 22\ R_E$.

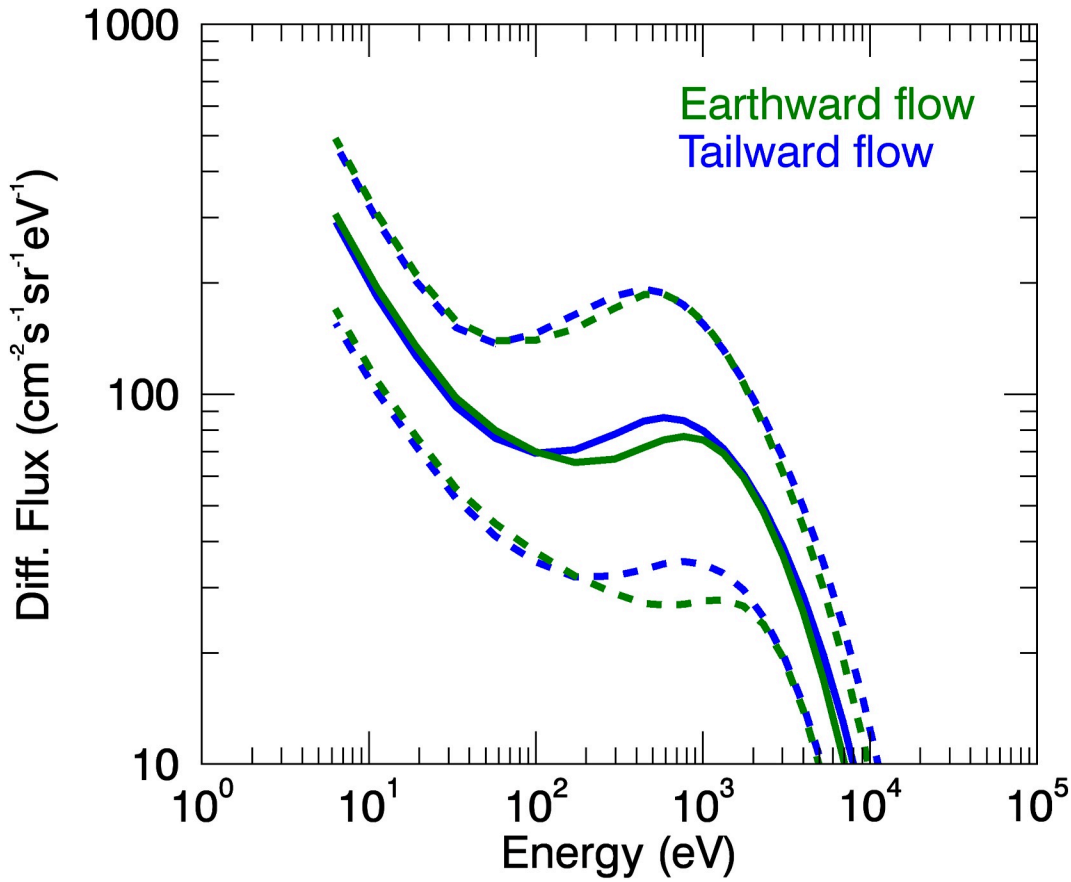

Figure 3. The differential energy spectra of the fluxes during earthward flow events (green) and the tailward flow events (blue). The solid lines indicate the 50th percentiles (medians) and the lower/upper dashed lines indicate 25th/75th percentiles (lower/upper quartiles).

Moreover, Liou et al. (2001) reported that auroral substorm onsets are more likely to occur in the pre-midnight sector auroral ionosphere. Their results indicate the formation of the near-Earth *X* line (neutral line) in the pre-midnight sector, which can explain why the tailward flow appears more frequently in the duskside for larger velocities (Figures 2h–2j).

To determine the number of protons implanted into the lunar surface to simulate both earthward and tailward flow implantation as model inputs, we proceeded by computing the median energy spectrum for both earthward and tailward flows (|Vx| > 30 km/s). Figure 3 shows the median (solid lines) and lower/upper quartiles (dashed lines) of the differential number fluxes (DNFs; in units of cm ^{2}s ^{1}sr ^{1} eV ^{1}) for ions observed during earthward flow events (green) and the tailward flow events (blue) as a function of the energy channel. By applying F 2π DNF dE (where F is the flux (in units of cm ^{2}s ^{1}), dE is the energy channel spacing (in units of eV), and 2π represents the solid angle (in units of sr) of the hemisphere for both the tailward and earthward flows) to the median values of DNF in different energy channels, we can obtain 1.73 10^{6} cm ^{2}s ^{1} and 1.94 10^{6} cm ^{2}s ^{1} as the fluxes for the earthward flow and tailward flow, respectively, in the statistical manner. Since their fluxes are basically at the same order of magnitude and each run of the model is 1 hr (update the lunar surface temperature each hour and record each water molecule condition), we used a population of 10,000 test particles per hour as proxies (the scaling factor is 1/360,000) for lunar water molecules produced by earthward/tailward ions due to limited computational resource constraints, so as to study the surface distribution of water molecules and their relative amounts on surface, in flight, and cold-trapped in polar regions. Subsequently, we assessed the total duration of these earthward and tailward flow events within the magnetotail. The total time duration of earthward flow events is 14 hr per month and that of the tailward flow events is 12 hr per month. The implantation time duration depends on the mean monthly time durations of the earthward and tailward flow events, which are

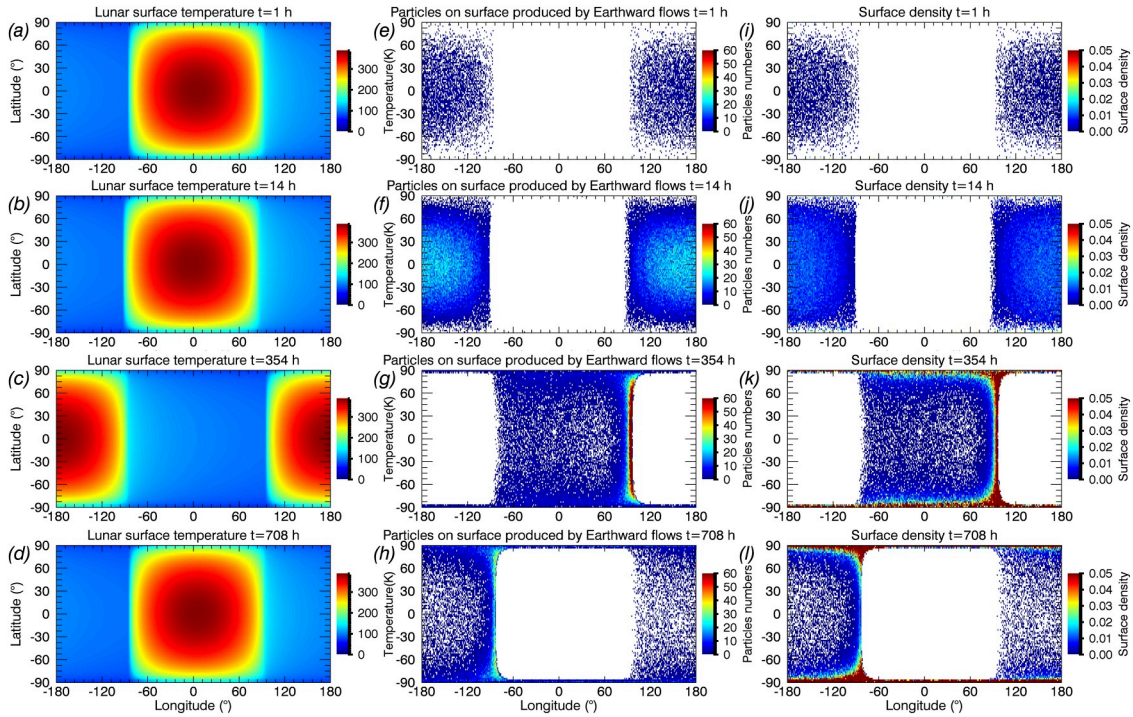

Figure 4. The model results of water molecules produced by earthward flows. (a–d) The lunar surface temperature, (e–f) the water molecules' distribution on the lunar surface, and (i–l) density of water molecules on the lunar surface at different times during 1 month.

estimated from the ARTEMIS observations. The water molecules are assumed to be continuously produced for 14 hr by earthward flows and 12 hr by tailward flows around the full moon lunar phase (GSM-Y equal to 0).

Based on the above results, we then substituted the ARTEMIS observations into the water molecular migration model to explore the possible influence of the earthward and tailward flows on the lunar surficial water. The number of water molecules was assumed according to the weights of the earthward flow and tailward flow energy flux. The earthward and tailward flows implanted on the lunar surface when the Moon is in the magnetotail at about $10\ R_E < Y_{\mathrm{GSM}} < 10\ R_E$ were set in the model. The earthward flow implantation time duration is set as 14 hr on the lunar farside surface, and tailward flow implantation time duration is set as 12 hr on the lunar nearside surface per month.

The distributions of lunar surface temperature and the water molecules implanted by the earthward and tailward flows within 1 month are shown in Figures 4 and 5. We assume that the Moon is a sphere with a radius of 1,738 km. The surface density is calculated by the number of water molecules divided by the lunar surface area in each grid cell. The first rows of Figures 4 and 5 show the initial temperature (Figures 4a and 5a), water molecules distribution (Figures 4e and 5e), and surface density (Figures 4i and 5i) of water molecules on the lunar surface when the Moon was just implanted by the earthward and tailward flows in the magnetotail in the first hour. The second row of Figures 4 and 5 are temperature (Figures 4b and 5b), water molecules distribution (Figures 4f and 5f), and surface density (Figures 4h and 5h) of water molecules on the lunar surface after the Moon is implanted for 14 and 12 hr by the earthward and tailward flows separately. We can find that most of the water molecules produced by the earthward flows are retained on the lunar surface, while the water molecules produced by the tailward flows migrate quickly to the morning and evening terminators. When the Moon is within the Earth's magnetotail, the lunar farside lies in the nighttime, resulting in an extremely low surface temperature. Consequently, water molecules generated by earthward flows possess insufficient energy to migrate to the exosphere and thus remain on the surface. However, the lunar nearside is on the dayside when the Moon is in the magnetotail, and the surface temperature on the lunar dayside is high enough to migrate water across the surface and the exosphere, resulting in the diffusive migration of water molecules to the morning and evening terminators.

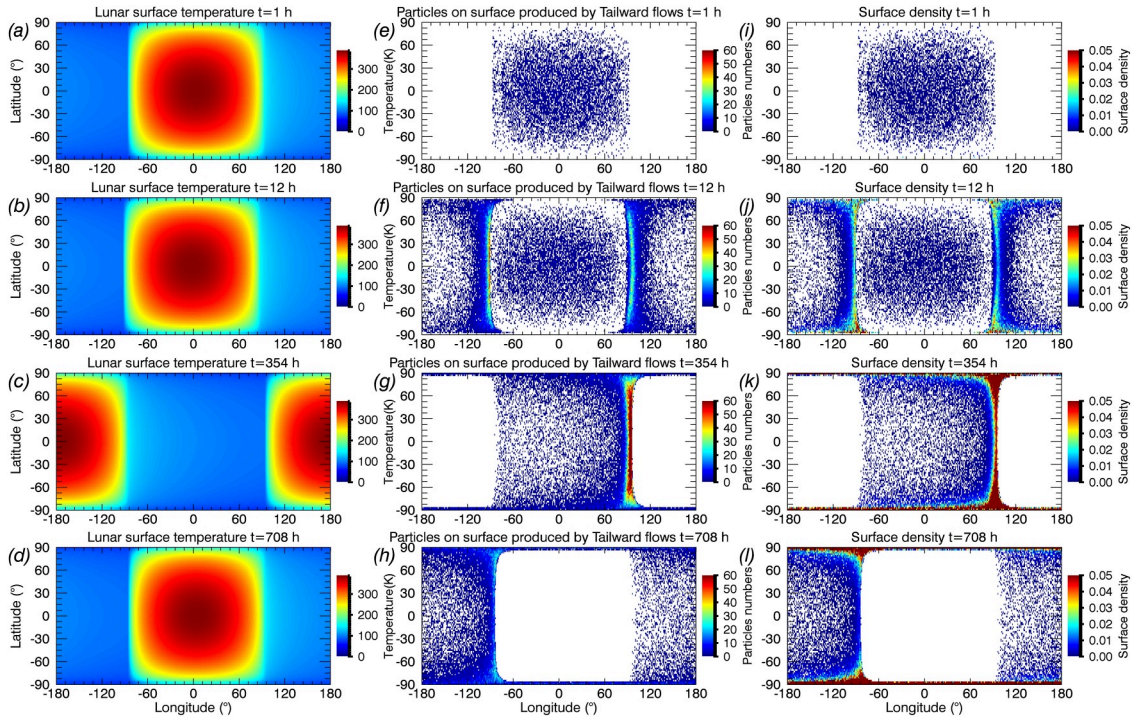

Figure 5. The model results of water molecules produced by tailward flows. (a–d) The lunar surface temperature, (e–f) the water molecules' distribution on the lunar surface, and (i–l) density of water molecules on the lunar surface at different times during 1 month.

When the lunar farside is illuminated by the Sun, the water molecules begin to migrate between the surface and exosphere. The lunar surface temperature (Figures 4c, 4d, 5c, and 5d), water molecule distributions (Figures 4g, 4h, 5g, and 5h), and surface density (Figures 4k, 4l, 5k, and 5l) after migration for half a month (354 hr) and one month (708 hr) are shown in the third panel and fourth rows of Figures 4 and 5. We can see that the water molecules produced by both earthward flows and tailward flows migrate to the higher-latitude regions and to the morning terminator, which is consistent with previous studies (Schörghofer et al., 2017).

The number of water molecules on the surface produced by earthward flows and tailward flows after migration for 1 month and 4 months are compared in Table 1. We find that the number of water molecules produced by earthward flows and remaining on the lunar surface are 28% higher than water molecules produced by tailward flows and remaining after 1-month and 4-month migration. This indicates that the water molecules produced by earthward flows have a higher probability of being preserved on the lunar surface even after the migration process.

When comparing the number of cold trapped water molecules produced by earthward flows and tailward flows, we find that water molecules produced by tailward flows and falling into the lunar polar cold traps are 13% higher than those produced by earthward flows and falling into the lunar polar cold traps after 1-month of

Table 1
The Number Distribution of the Water Molecules Produced by the Earthward Flows and the Tailward Flows After Migration for One Month and Four Months

Water molecular produced by	Time interval	On surface	In-flight	Cold trapped-north	Cold trapped-south	Destroyed	Particles produced
Earthward flow	14h	139,795	151	2	1	51	140,000
Tailward flow	12h	53,913	45,738	404	520	19,425	120,000
Earthward flow	1 month	37,132	1,203	3,937	4,547	93,181	140,000
Tailward flow	1 month	26,935	686	4,509	5,095	82,775	120,000
Earthward flow	4 months	50,406	1,524	26,799	30,304	460,967	560,000
Tailward flow	4 months	36,217	890	25,660	28,868	388,365	480,000

migration. The water molecules produced by the tailward flows migrating into cold trapped regions are more than those produced by the earthward flows, which indicates that the water molecules transport is more intense on the lunar nearside due to the higher temperature at that time. However, the water molecules produced by the earthward flows migrating into cold trapped regions increase after 4-months of migration because of the accumulation of the water molecules produced by earthward flows. By comparing the water molecules in southern/northern cold-trapped regions, we find that the water molecules in the southern cold trapped region are more than those in the northern cold trapped regions because the areal coverage of cold traps is higher in the southern polar regions of the Moon.

5. Discussion

In this study, we focus on the lateral transport of water molecules produced by the earthward and tailward flows. In addition to the earthward flows, high-energy protons and heavier ions in the tailward flow will also possibly implant into the lunar farside because of their large gyro radii. The Earth wind contains a large number of high-energy protons and heavy ions. And there are large variations in the energy flux spectra between and within different flow events. The energy flux at energies higher than 4 keV is larger in earthward/tailward flow than that in the solar wind. Schaible and Baragiola (2014) have shown in a laboratory experiment that at three specific proton energies of 2, 5, and 10 keV hydrogen into silica and silicates, higher energy protons can produce more OH species, and this increase was quantified as a function of fluence. This is because the high energy protons could penetrate more deeply into the material. When comparing the column density after implanting the same fluence of hydrogen, it is observed that the column density in olivine is notably greater than that in amorphous SiO_2, which is implanted at the same energy level. This disparity is likely attributed to the fact that in the olivine crystal enables the hydrogen ions to penetrate more deeply into the material. This suggests that the shape of the energy spectrum could possibly influence the production rate of water molecules. However, the effect and physical mechanism of energetic particles and heavy ions or high-energy electrons on lunar water formation need to be further explored by particle irradiation experiments and simultaneous observations of lunar surface water and ambient plasma fluxes, to find conclusive evidence in one way or the other.

The information of the evolution history of the geomagnetic dipole could be recorded in the lunar farside (Wei et al., 2020). Prior to the Earth's development of a dipolar magnetic field, upper atmospheric ions might continuously escape into the interplanetary space as a result of solar wind interaction with the Earth's ionosphere. At that time, the Earth's atmospheric ions could only implant into the lunar nearside. When the Earth's magnetosphere formed, the near *X*-line is typically located at 20–30 Re from the Earth and the distant *X*-line is located at around 120 Re from the Earth. The Moon enters the magnetosphere at 60 Re, which is in the middle of two *X*-lines where the lunar nearside soil will be implanted by the tailward flows produced from the near *X*-line, and the lunar farside soil will be implanted by the earthward flows produced from the distant *X*-line. In this case, the lunar soil should have been impacted by the Earth's atmospheric ions on both the nearside and farside. In addition, the total time duration of earthward flow events is 14 hr per month, while that of the tailward flow events is 12 hr per month was examined in this study. The continuous and long-term implantation of the earthward flow onto the lunar farside is likely to have persisted for the past several billion years. Thus, it is possible to constrain the evolution history of Earth's magnetic field and atmospheric composition if a historical profile of those Earth's atmospheric ions could be acquired from the lunar farside soils.

More recently, many studies have shown that the Earth's atmospheric ions were observed near the Moon. Using Kaguya observations, Terada et al. (2017) discovered that relatively high-energy (1–10 keV) O ions appear only when the Moon and Kaguya cross the plasma sheet and the lunar soil oxygen isotope ratios are well explained by these O ions from Earth's atmosphere. Yamauchi et al. (2024) observed low-energy (below 1 keV) O ions from the Earth and suggested that these ions have a non-negligible impact on the ion composition and the ion mass density in the lunar plasma environment. Using the ARTEMIS observations, Poppe et al. (2016) observed terrestrial ions in the Earth's magnetotail. Barani et al. (2024) proposed that the heavy ion population mainly consists of O ions with velocities 25% more than the velocity of the concurrently observed protons at the lunar distances. In addition, Zong et al. (1998) found earthward bursts of energetic oxygen ions in the magnetotail using the Geotail satellite observations. The occurrence rate of these energetic oxygen ions is higher when a magnetic storm occurs (Fu & Zong, 2006; Yue et al., 2018, 2019). These observations reveal that the plasma flows containing heavy ions could reach both the nearside and farside of the Moon.

The penetration or implantation depth into lunar soil grains primarily depends on the energy of the incident ions, the angle of incidence, and the target surface composition. For example, this depth is typically 20 nm for 1 keV protons and 30–40 nm for 10 keV O ions (Farrell et al., 2017; Terada et al., 2017). The energy of particles in the earthward and tailward flows is higher than that in the solar wind. Part of these particles generate water that migrates to the polar regions. Additionally, some of the particles remain in the lunar soil because high-energy protons and heavy ions can implant deeper into the lunar soil. We find that the occurrence rate of the earthward flows is generally higher than the tailward flows when low velocities are included. However, the occurrence rate of the tailward flows is higher when |Vx| is greater than 400 km/s. The velocities between the earthward flows and tailward flows are different. For the two kinds of flow speed, the implantation depths of the same ion species energy difference are significantly different. The isotope compositions of the implanted plasma particles can be deduced by analyzing the outermost implanted layer of a single lunar soil grain. Meanwhile, the exposure ages of soil grain can be ascertained through an examination of its interior part (Ozima et al., 2008). Therefore, the comprehensive isotopic analyses of soil grains from the lunar farside in the laboratory will provide decisive evidence for whether the Earth's atmospheric ions could reach the farside of the Moon and deduce the evolution history of the geomagnetic dipole.

6. Conclusions

In conclusion, we have investigated the possible influence of earthward flow and tailward flow events on the lunar surficial water by using the ARTEMIS observations from January 2011 to January 2022 and a Monte Carlo model. The occurrence rate distribution of the earthward/tailward flows (determined by $Vx > 30$ km/s or $Vx < 30$ km/s) in the plasma sheet has been examined. The median energy spectra of the earthward/tailward flows were calculated. The number of water molecules was assumed according to the weights of the earthward flow and tailward flow energy flux. The occurrence position, the time duration, and the number of water molecules produced by earthward flows and tailward flows were given by the ARTEMIS observations. We then simulate the different influences of the earthward flow and tailward flow events on the lunar water molecules according to a Monte Carlo model. The water molecules produced by the earthward flows implanted into the lunar farside surface show higher stability due to the lower temperature in the nightside. The earthward flows could produce more water on the lunar farside surface, which could migrate more to cold traps compared to the tailward flows after a long accumulation time. The magnetotail can be used as a bridge between a planet and its moons, and the accelerated planetary atmospheric ions into space may be implanted and preserved on its moon's surface. This work gives a clue that the Moon's farside could record more information about the planet itself and provides strong motivation for the sample return missions to the lunar farside, such as the Chang'E-6 mission.

Conflict of Interest

The authors declare no conflicts of interest relevant to this study.

Data Availability Statement

The ARTEMIS data are available at http://artemis.ssl.berkeley.edu. Model source code that includes the detailed equations is available in Schörghofer (2024), and simulation data analyzed in this manuscript are archived and accessible in Wang et al. (2025).

Acknowledgments
We thank all the members of the ARTEMIS instrument teams and N. Schörghofer's Model. This work was supported by the National Natural Science Foundation of China (Grants 42225405, 42304185, and 42304172) and Shandong Provincial Natural Science Foundation (ZR2023ZD36 and ZR2023QD119), the Specialized Research Fund for State Key Laboratory of Solar Activity and Space Weather, and the High-End Foreign Expert Introduction Plan of China.

References

Angelopoulos, V. (2011). The ARTEMIS mission. *Space Science Reviews*, *165*(1–4), 3–25. https://doi.org/10.1007/s11214-010-9687-2

Angelopoulos, V., Baumjohann, W., Kennel, C. F., Coroniti, F. V., Kivelson, M. G., Fellat, R., et al. (1992). Bursty bulk flows in the inner central plasma sheet. *Journal of Geophysical Research*, *97*(A4), 4027–4039. https://doi.org/10.1029/91ja02701

Angelopoulos, V., Kennel, C. F., Coroniti, F. V., Pellat, R., Kivelson, M. G., Walker, R. J., et al. (1994). Statistical characteristics of bursty bulk flow events. *Journal of Geophysical Research*, *99*(A11), 21257–21280. https://doi.org/10.1029/94ja01263

Artemyev, A. V., Angelopoulos, V., Runov, A., & Vasko, I. Y. (2017). Hot ion flows in the distant magnetotail: ARTEMIS observations from lunar orbit to 200 RE. *Journal of Geophysical Research: Space Physics*, *122*(10), 9898–9909. https://doi.org/10.1002/2017JA024433

Auster, H. U., Glassmeier, K. H., Magnes, W., Aydogar, O., Baumjohann, W., Constantinescu, D., et al. (2008). The THEMIS fluxgate magnetometer. *Space Science Reviews*, *141*(1–4), 235–264. https://doi.org/10.1007/s11214-008-9365-9

Bandfield, J. L., Poston, M. J., Klima, R. L., & Edwards, C. S. (2018). Widespread distribution of OH/H_2O on the lunar surface inferred from spectral data. *Nature Geoscience*, *11*(3), 173–177. https://doi.org/10.1038/s41561-018-0065-0

Barani, M., Poppe, A. R., Fillingim, M. O., McFadden, J. P., Halekas, J. S., & Sibeck, D. G. (2024). A study of ionospheric heavy ions in the terrestrial magnetotail using ARTEMIS. *Journal of Geophysical Research*, *129*(6), e2023032346. https://doi.org/10.1029/2023JA032346

Baumjohann, W., Paschmann, G., & Lühr, H. (1990). Characteristics of high-speed ion flows in the plasma sheet. *Journal of Geophysical Research*, *95*(A4), 3801. https://doi.org/10.1029/ja095ia04p03801

Butler, B. J. (1997). The migration of volatiles on the surfaces of Mercury and the Moon. *Journal of Geophysical Research*, *102*(E8), 19283–19291. https://doi.org/10.1029/97JE01347

Cao, J. B., Ma, Y. D., Parks, G., Reme, H., Dandouras, I., Nakamura, R., et al. (2006). Joint observations by cluster satellites of bursty bulk flows in the magnetotail. *Journal of Geophysical Research*, *111*(A4), A04206. https://doi.org/10.1029/2005JA011322

Chong, G. S., Pitkänen, T., Hamrin, M., & Kullen, A. (2022). Dawn-dusk ion flow asymmetry in the plasma sheet: Interplanetary magnetic field B_y versus distance with respect to the neutral sheet. *Journal of Geophysical Research: Space Physics*, *127*(4), e2021JA030208. https://doi.org/10.1029/2021JA030208

Crider, D. H., & Vondrak, R. R. (2000). The solar wind as a possible source of lunar polar hydrogen deposits. *Journal of Geophysical Research*, *105*(E11), 26773–26782. https://doi.org/10.1029/2000JE001277

Crider, D. H., & Vondrak, R. R. (2002). Hydrogen migration to the lunar POLES by solar wind bombardment of the moon. *Advances in Space Research*, *30*(8), 1869–1874. https://doi.org/10.1016/s0273-1177(02)00493-3

Crovisier, J. (1989). The photodissociation of water in cometary atmospheres. *Astronomy and Astrophysics*, *213*, 459–464.

Djouadi, Z., Robert, F., le Sergeant D'Hendecourt, L., Mostefaoui, S., Leroux, H., Jones, A. P., & Borg, J. (2011). Hydroxyl radical production and storage in analogues of amorphous interstellar silicates: A possible "wet" accretion phase for inner telluric planets. *Astronomy and Astrophysics*, *531*, A96. https://doi.org/10.1051/0004-6361/201116722

Farrell, W. M., Hurley, D. M., Esposito, V. J., McLain, J. L., & Zimmerman, M. I. (2017). The statistical mechanics of solar wind hydroxylation at the Moon, within lunar magnetic anomalies, and at Phobos. *Journal of Geophysical Research: Planets*, *122*(1), 269–289. https://doi.org/10.1002/2016JE005168

Fu, S. Y., Wilken, B., Zong, Q. G., & Pu, Z. Y. (2001). Ion composition variations in the inner magnetosphere: Individual and collective storm effects in 1991. *Journal of Geophysical Research*, *106*(A12), 29683–29704. https://doi.org/10.1029/2000ja900173

Fu, S. Y., & Zong, Q.-G. (2006). Energetic particle composition signatures in the Earth magnetotail. *Advances in Geosciences*, *2*, 143–161. Volume 2: Solar Terrestrial (ST). https://doi.org/10.1142/9789812707185_0012

Gencturk Akay, I., Kaymaz, Z., & Sibeck, D. G. (2019). Magnetotail boundary crossings at lunar distances: ARTEMIS observations. *Journal of Atmospheric and Solar-Terrestrial Physics*, *182*, 45–60. https://doi.org/10.1016/j.jastp.2018.11.002

Harnett, E. M., Cash, M., & Winglee, R. M. (2013). Substorm and storm time ionospheric particle flux at the Moon while in the terrestrial magnetosphere. *Icarus*, *224*(1), 218–227. https://doi.org/10.1016/j.icarus.2013.02.022

Hendrix, A. R., Hurley, D. M., Farrell, W. M., Greenhagen, B. T., Hayne, P. O., Retherford, K. D., et al. (2019). Diurnally migrating lunar water: Evidence from ultraviolet data. *Geophysical Research Letters*, *46*(5), 2417–2424. https://doi.org/10.1029/2018gl081821

Honniball, C. I., Lucey, P. G., Li, S., Shenoy, S., Orlando, T. M., Hibbitts, C. A., et al. (2021). Molecular water detected on the sunlit Moon by SOFIA. *Nature Astronomy*, *5*(2), 121–127. https://doi.org/10.1038/s41550-020-01222-x

Ichimura, A. S., Zent, A. P., Quinn, R. C., Sanchez, M. R., & Taylor, L. A. (2012). Hydroxyl (OH) production on airless planetary bodies: Evidence from H /D ion-beam experiments. *Earth and Planetary Science Letters*, *345–348*, 90–94. https://doi.org/10.1016/j.epsl.2012.06.027

Kiehas, S. A., Runov, A., Angelopolos, V., Hietala, H., & Korovinksiy, D. (2018). Magnetotail fast flow occurrence rate and dawn-dusk asymmetry at XGSM 60 RE. *Journal of Geophysical Research: Space Physics*, *123*(3), 1767–1778. https://doi.org/10.1002/2017JA024776

Kissinger, J., McPherron, R. L., Hsu, T.-S., & Angelopoulos, V. (2012). Diversion of plasma due to high pressure in the inner magnetosphere during steady magnetospheric convection. *Journal of Geophysical Research*, *117*(A5), A05206. https://doi.org/10.1029/2012JA017579

Kramer, G. Y., Besse, S., Dhingra, D., Nettles, J., Klima, R., Garrick-Bethell, I., et al. (2011). M3 spectral analysis of lunar swirls and the link between optical maturation and surface hydroxyl formation at magnetic anomalies. *Journal of Geophysical Research*, *116*(9), E00G18. https://doi.org/10.1029/2010JE003729

Li, S., & Garrick Bethell, I. (2019). Surface water at lunar magnetic anomalies. *Geophysical Research Letters*, *46*(24), 14318–14327. https://doi.org/10.1029/2019gl084890

Li, S., & Milliken, R. E. (2017). Water on the surface of the Moon as seen by the Moon mineralogy mapper: Distribution, abundance, and origins. *Science Advances*, *3*(9), e1701471. https://doi.org/10.1126/sciadv.1701471

Li, S., Poppe, A. R., Orlando, T. M., Jones, B. M., Tucker, O. J., Farrell, W. M., & Hendrix, A. R. (2023). Formation of lunar surface water associated with high-energy electrons in Earth's magnetotail. *Nature Astronomy*, *7*(12), 1427–1435. https://doi.org/10.1038/s41550-023-02081-y

Liou, K., Newell, P. T., Sibeck, D. G., Meng, C.-I., Brittnacher, M., & Parks, G. (2001). Observation of IMF and seasonal effects in the location of auroral substorm onset. *Journal of Geophysical Research*, *106*(A4), 5799–5810. https://doi.org/10.1029/2000JA003001

Liuzzo, L., Poppe, A. R., & Halekas, J. S. (2022). A statistical study of the moon's Magnetotail plasma environment. *Journal of Geophysical Research: Space Physics*, *127*(4), e2022JA030260. https://doi.org/10.1029/2022JA030260

Lu, S., Lin, Y., Angelopoulos, V., Artemyev, A. V., Pritchett, P. L., Lu, Q., & Wang, X. Y. (2016). Hall effect control of magnetotail dawn-dusk asymmetry: A three-dimensional global hybrid simulation. *Journal of Geophysical Research: Space Physics*, *121*(12), 11882–11895. https://doi.org/10.1002/2016JA023325

Ma, Y., Wong, H.-C., & Xu, X. (2015). Subsonic and sunward-orientated lunar wake observed by ARTEMIS in the geomagnetotail. *Astrophysics and Space Science*, *358*(2), 34. https://doi.org/10.1007/s10509-015-2430-4

McCord, T. B., Taylor, L. A., Combe, J. P., Kramer, G., Pieters, C. M., Sunshine, J. M., & Clark, R. N. (2011). Sources and physical processes responsible for OH/H_2O in the lunar soil as revealed by the Moon Mineralogy Mapper (M^3). *Journal of Geophysical Research*, *116*(4), E00G05. https://doi.org/10.1029/2010JE003711

McFadden, J. P., Carlson, C. W., Larson, D., Ludlam, M., Abiad, R., Elliott, B., et al. (2008). The THEMIS ESA plasma instrument and In-flight calibration. *Space Science Reviews*, *141*(1–4), 277–302. https://doi.org/10.1007/s11214-008-9440-2

Nagai, T., Fujimoto, M., Saito, Y., Machida, S., Terasawa, T., Nakamura, R., et al. (1998). Structure and dynamics of magnetic reconnection for substorm onsets with geotail observations. *Journal of Geophysical Research*, *103*(A3), 4419–4440. https://doi.org/10.1029/97ja02190

Ozima, M., Seki, K., Terada, N., Miura, Y. N., Podosek, F. A., & Shinagawa, H. (2005). Terrestrial nitrogen and noble gases in lunar soils. *Nature*, *436*(7051), 655–659. https://doi.org/10.1038/nature03929

Ozima, M., Yin, Q. Z., Podosek, F. A., & Miura, Y. N. (2008). Toward understanding early Earth evolution: Prescription for approach from terrestrial noble gas and light element records in lunar soils. *Proceedings of the National Academy of Sciences*, *105*(46), 17,654–17,658. https://doi.org/10.1073/pnas.0806596105

Pieters, C. M., Goswami, J. N., Clark, R. N., Annadurai, M., Boardman, J., Buratti, B., et al. (2009). Character and spatial distribution of OH/H_2O on the surface of the moon seen by M^3 on Chandrayaan-1. *Science*, *326*(5952), 568–572. https://doi.org/10.1126/science.1178658

Pitkänen, T., Hamrin, M., Karlsson, T., Nilsson, H., & Kullen, A. (2017). *On IMF* B $_y$ -induced dawn-dusk asymmetries in earthward convective fast flows (pp. 95–106). https://doi.org/10.1002/9781119216346.ch8

Pitkänen, T., Kullen, A., Laundal, K. M., Tenfjord, P., Shi, Q. Q., Park, J.-S., et al. (2019). IMF B_y influence on magnetospheric convection in Earth's magnetotail plasma sheet. *Geophysical Research Letters*, *46*(21), 11698–11708. https://doi.org/10.1029/2019GL084190

Poppe, A. R., Farrell, W. M., & Halekas, J. S. (2018). Formation timescales of amorphous rims on lunar grains derived from ARTEMIS observations. *Journal of Geophysical Research: Planets*, *123*(1), 37–46. https://doi.org/10.1002/2017JE005426

Poppe, A. R., Fillingim, M. O., Halekas, J. S., Raeder, J., & Angelopoulos, V. (2016). ARTEMIS observations of terrestrial ionospheric molecular ion outflow at the Moon. *Geophysical Research Letters*, *43*(13), 6749–6758. https://doi.org/10.1002/2016GL069715

Schaible, M. J., & Baragiola, R. A. (2014). Hydrogen implantation in silicates: The role of solar wind in SiOH bond formation on the surfaces of airless bodies in space. *Journal of Geophysical Research: Planets*, *119*(9), 2017–2028. https://doi.org/10.1002/2014JE004650

Schörghofer, N. (2014). Migration calculations for water in the exosphere of the Moon: Dusk-dawn asymmetry, heterogeneous trapping, and D/H fractionation. *Geophysical Research Letters*, *41*(14), 4888–4893. https://doi.org/10.1002/2014GL060820

Schörghofer, N. (2024). *Planetary-code-Collection: Thermal, ice evolution, and exosphere models for planetary surfaces (version v1.2.2)*. Zenodo. https://doi.org/10.5281/ZENODO.10583245

Schörghofer, N., Lucey, P., & Williams, J. P. (2017). Theoretical time variability of mobile water on the Moon and its geographic pattern. *Icarus*, *298*, 111–116. https://doi.org/10.1016/j.icarus.2017.01.029

Seki, K., Elphic, R. C., Hirahara, M., Terasawa, T., & Mukai, T. (2001). On atmospheric loss of oxygen ions from Earth through magnetospheric processes. *Science*, *291*(5510), 1–4. https://doi.org/10.1126/science.1058913

Sibeck, D. G., Angelopoulos, V., Brain, D. A., Delory, G. T., Eastwood, J. P., Farrell, W. M., et al. (2011). ARTEMIS science objectives. *Space Science Reviews*, *165*(1–4), 59–91. https://doi.org/10.1007/s11214-011-9777-9

Sunshine, J. M., Farnham, T. L., Feaga, L. M., Groussin, O., Merlin, F., Milliken, R. E., & A'Hearn, M. F. (2009). Temporal and spatial variability of lunar hydration as observed by the Deep impact spacecraft. *Science*, *326*(5952), 565–568. https://doi.org/10.1126/science.1179788

Tang, H., Wang, S., & Li, X. (2012). Simulation of nanophase iron production in lunar space weathering. *Planetary and Space Science*, *60*(1), 322–327. https://doi.org/10.1016/j.pss.2011.10.006

Terada, K., Yokota, S., Saito, Y., Kitamura, N., Asamura, K., & Nishino, M. N. (2017). Biogenic oxygen from Earth transported to the Moon by a wind of magnetospheric ions. *Nature Astronomy*, *1*(2), 0026. https://doi.org/10.1038/s41550-016-0026

Vasavada, A. R., Bandfield, J. L., Greenhagen, B. T., Hayne, P. O., Siegler, M. A., Williams, J., & Paige, D. A. (2012). Lunar equatorial surface temperatures and regolith properties from the Diviner Lunar Radiometer Experiment. *Journal of Geophysical Research*, *117*(E12). https://doi.org/10.1029/2011JE003987

Wang, H., Shi, Q., & Zhang, J. (2025). Influence of the earthward and tailward ion flows on the lunar surface water in the magnetotail [Dataset]. *Zenodo*. https://doi.org/10.5281/zenodo.14994436

Wang, H. Z., Zhang, J., Shi, Q. Q., Saito, Y., Degeling, A. W., Rae, I. J., et al. (2021). Earth wind as a possible exogenous source of lunar surface hydration. *The Astrophysical Journal*, *907*(2), L32. https://doi.org/10.3847/2041-8213/abd559

Watson, K., C. Murray, B., & Brown, H. (1961). The behavior of volatiles on the lunar surface. *Journal of Geophysical Research*, *66*(9), 3033–3045. https://doi.org/10.1029/jz066i009p03033

Wei, Y., Pu, Z., Zong, Q., Wan, W., Ren, Z., Fraenz, M., et al. (2014). Oxygen escape from the Earth during geomagnetic reversals: Implications to mass extinction. *Earth and Planetary Science Letters*, *394*, 94–98. https://doi.org/10.1016/j.epsl.2014.03.018

Wei, Y., Zhong, J., Hui, H., Shi, Q., Cui, J., He, H., et al. (2020). Implantation of Earth's atmospheric ions into the nearside and farside lunar soil: Implications to geodynamo evolution. *Geophysical Research Letters*, *47*(3), e2019GL086208. https://doi.org/10.1029/2019gl086208

Wöhler, C., Grumpe, A., Berezhnoy, A. A., & Shevchenko, V. V. (2017). Time-of-day-dependent global distribution of lunar surficial water/hydroxyl. *Science Advances*, *3*(9), e1701286. https://doi.org/10.1126/sciadv.1701286

Yamauchi, D., Nosé, M., Harada, Y., Yamamoto, K., Keika, K., Nagamatsu, A., et al. (2024). Terrestrial-origin O ions below 1 keV near the Moon measured with the Kaguya satellite. *Earth Planets and Space*, *76*, 162. https://doi.org/10.1186/s40623-024-02107-3

Yue, C., Bortnik, J., Li, W., Ma, Q., Gkioulidou, M., Reeves, G. D., et al. (2018). The composition of plasma inside geostationary orbit based on Van Allen probes observations. *Journal of Geophysical Research: Space Physics*, *123*(8), 6478–6493. https://doi.org/10.1029/2018JA025344

Yue, C., Bortnik, J., Li, W., Ma, Q., Wang, C., Thorne, R. M., et al. (2019). Oxygen ion dynamics in the Earth's ring current: Van Allen probes observations. *Journal of Geophysical Research: Space Physics*, *124*(10), 7786–7798. https://doi.org/10.1029/2019JA026801

Zeng, X., Tang, H., Li, X. Y., Zeng, X., Yu, W., Liu, J., & Zou, Y. (2021). Experimental investigation of OH/H_2O in H -irradiated plagioclase: Implications for the thermal stability of water on the lunar surface. *Earth and Planetary Science Letters*, *560*, 116806. https://doi.org/10.1016/j.epsl.2021.116806

Zhang, L. Q., Baumjohann, W., Wang, C., Dai, L., & Tang, B. B. (2016). Bursty bulk flows at different magnetospheric activity levels: Dependence on IMF conditions. *Journal of Geophysical Research: Space Physics*, *121*(9), 8773–8789. https://doi.org/10.1002/2016JA022397

Zhang, L. Q., Baumjohann, W., Wang, J. Y., Rème, H., Dunlop, M. W., & Chen, T. (2015). Statistical characteristics of slow earthward and tailward flows in the plasma sheet. *Journal of Geophysical Research: Space Physics*, *120*(8), 6199–6206. https://doi.org/10.1002/2015JA021354

Ziegler, J. F., Ziegler, M. D., & Biersack, J. P. (2010). SRIM – The stopping and range of ions in matter (2010). *Nuclear Instruments and Methods in Physics Research Section B: Beam Interactions with Materials and Atoms*, *268*(11–12), 1818–1823. https://doi.org/10.1016/j.nimb.2010.02.091

Zong, Q. G., Wilken, B., Woch, J., Mukai, T., Yamamoto, T., Reeves, G. D., et al. (1998). Energetic oxygen ion bursts in the distant magnetotail as a product of intense substorms: Three case studies. *Journal of Geophysical Research*, *103*(A9), 20339–20363. https://doi.org/10.1029/97JA01146